Pergamon

Int. J. Mach. Tools Manufact. Vol. 36, No. 9, pp. 1059–1072, 1996

0890-6955/96$15.00 + .00

0890-6955(95)00081-X

PREDICTION OF BALL-END MILLING FORCES FROM ORTHOGONAL CUTTING DATA

P. LEE† and Y. ALTINTAŞ*†

(*Original received* 11 *April* 1995)

Abstract—The mechanics of cutting with helical ball-end mills are presented. The fundamental cutting parameters, the yield shear stress, average friction coefficient on the rake face and shear angle are measured from a set of orthogonal cutting tests at various cutting speeds and feeds. The cutting forces are separated into edge or ploughing forces and shearing forces. The helical flutes are divided into small differential oblique cutting edge segments. The orthogonal cutting parameters are carried to oblique milling edge geometry using the classical oblique transformation method, where the chip flow angle is assumed to be equal to the local helix angle. The cutting force distribution on the helical ball-end mill flutes is accurately predicted by the proposed method, and the model is validated experimentally and statistically by conducting more than 60 ball-end milling experiments.

NOMENCLATURE

a	axial depth of cut
b	width of cut
F_P, F_Q	power and thrust force components in orthogonal cutting
F_{xj}, F_{yj}, F_{zj}	milling forces in Cartesian coordinates on flute j
dF_t, dF_r, dF_a	differential cutting forces in tangential, radial and axial direction in milling
i_0	helix angle at flute, shank meeting point
$i(\psi)$	local helix angle or angle of obliquity
ψ	lag angle between the tip (z=0) and a point on the helical flute at height z
Ψ	lag angle in global coordinate, measured from+y-axis CW
ψ_0	maximum lag angle between the tip (z=0) and uppermost cutting point (z=a)
K_{tc}, K_{rc}, K_{ac}	tangential, radial and axial cutting force coefficients in milling
K_{te}, K_{re}, K_{ae}	tangential, radial and axial edge force coefficients in milling
N_f	number of flutes
R_0	ball radius
$R(\psi)$	tool radius in x–y plane at a point defined by ψ
r_t	cutting chip ratio in orthogonal cutting
s_t	feed per tooth
t, t_c	uncut and cut chip thickness in orthogonal cutting
t_n	uncut chip thickness normal to cutting edge in milling
α_r, α_n	radial and normal rake angles
db	differential cutting edge length in the direction perpendicular to the cutting velocity
dz	differential length in axial direction
κ	angle in a vertical plane between a point on the flute and the z-axis
β	friction angle on the rake face
ϕ	shear angle in orthogonal cutting
ϕ_n, β_n	normal shear and normal friction angles in oblique cutting
η_c	chip flow angle on the rake face
τ	shear stress at the shear plane
θ	tool rotation angle, measured from+y-axis CW
ψ_1, ψ_2	integration limits
N	spindle speed in rpm

1. INTRODUCTION

Ball-end milling has been used extensively in the manufacturing of free form surfaces such as those encountered on dies and molds, turbines, propellers and aircraft structural components. The aerospace parts are usually made of high strength materials containing

*Author to whom correspondence should be addressed.
†Department of Mechanical Engineering, The University of British Columbia, Vancouver, British Columbia, Canada V6T 1Z4.

titanium, nickel and aluminum alloys and their precision and efficiency are critical in such operations.

Prior knowledge of cutting forces can assist process planners in selecting appropriate cutting conditions to reduce excessive tool wear or breakage and, more importantly, tool deflection which affects the quality of the finished parts. The traditional mechanistic approach is often used in predicting the cutting forces, where the cutting coefficients are identified through empirical curve fit to measured average milling forces [1]. Yucesan and Altintaş presented a semi-mechanistic model which predicts the shear and friction load distribution on the rake and flank faces of the helical ball-end mill flutes [2]. They predicted the cutting forces very accurately, but at the expense of conducting large number of ball-end milling experiments and using a complex mathematical model. The mechanistic models require large amount of milling tests, and are applicable to a particular workpiece material-cutter pair only. It will neither be practical nor useful in the case of a ball-end mill due to its complex geometry such as variable helix and rake angles. Yang and Park assumed that the ball-end mill geometry can be represented by segments of orthogonal cutting planes [3, 4]. They obtained the fundamental cutting parameters from orthogonal cutting tests and considered the variation in the chip loads due to static tool deflections. Tai and Fuh [5] used a similar cutting model, but they represented the cutting edge geometry as intersections between skew planes and spherical ball-end mill surface. Budak *et al.* presented a unified mechanics of cutting approach in predicting the milling force coefficients for cylindrical helical end mills [6]. They showed an accurate method of transformation between the orthogonal cutting parameters (i.e. shear stress, shear and friction angles) and local milling force coefficients.

In this paper, the unified mechanics model [6, 7] is extended to the helical ball-end mill geometry. The ball-end mill geometry is modelled analytically similar to those presented by Yucesan and Altintaş [2] and Ramaraj [8]. The flute is expressed in a parametric form and divided into small oblique cutting edges. Then mathematical relationships are developed to relate the geometry of each elemental oblique cut to the conventional practical machining variables obtained from orthogonal cutting tests. Process dependent cutting force coefficients are obtained from the orthogonal cutting data base. The linear flank edge force components, which constitute a significant part of the total forces in ball-end milling close to the ball tip region, are modelled and separated from shearing forces. The model is verified by conducting over 60 ball-end milling tests at different feeds, speeds, axial and radial depth of cuts and ball-end mill geometry. Statistical and sample time domain simulation results show that the approach can predict cutting forces accurately for any ball-end mill geometry and cutting conditions. A titanium alloy, an aerospace alloy which is considered difficult to machine, is used as a workpiece material.

Henceforth the paper is organized as follows. The geometric modelling of the ball-end mill cutters and ball-shaped helical flutes are presented in section 2. The modelling of cutting force expressions is shown in section 3, and followed by a cutting coefficients identification procedure in section 4. Experimental and simulation results are presented in section 5, and the paper is concluded with a summary of the proposed model in section 6.

2. GEOMETRIC MODEL OF A BALL-END MILL

The detailed geometry of a helical ball-end milling cutter is shown in Fig. 1(a)–(d). Each flute lies on the surface of the hemisphere, and is ground with a constant helix lead. The flutes have a helix angle of i_0 at the ball-shank meeting boundary [(Fig. 1(a)]. Due to the reduction of the radius at the x–y planes towards the ball tip in the axial (z) direction, the local helix angle $i(\psi)$ along the cutting flute varies for constant helix-lead cutters. The expression for the envelope of the ball part is given by

$$x^2 + y^2 + (R_0 - z)^2 = R_0^2 \tag{1}$$

where R_0 is the ball radius of the cutter measured from the center of the sphere (C). The cutter radius in the x–y plane at axial location z is

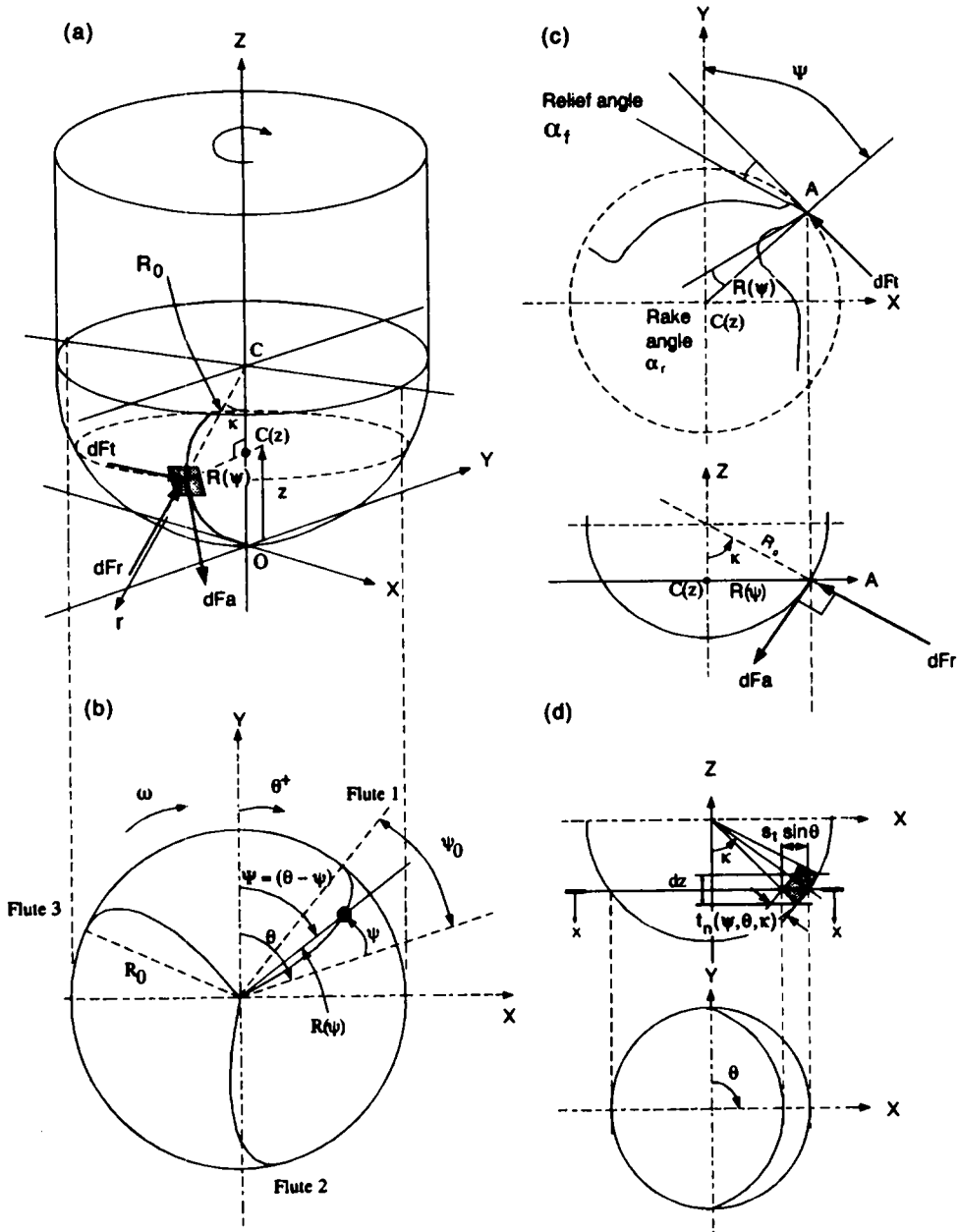

Fig. 1. Geometry and tool coordinates for a ball milling cutter.

$$R^2(z) = x^2 + y^2 \tag{2}$$

and it is zero at the ball tip. The z-coordinate of a point located on the cutting edge is

$$z = \frac{R_0 \psi}{\tan i_0} \tag{3}$$

where ψ is the lag angle between the tip of the flute at $z = 0$ and at axial location z, and it is due to the helix angle. ψ is measured clockwise from the+y-axis, see Fig. 1(b). The centre of the local coordinate system coincides with the global coordinate system X–Y–Z on the dynamometer shown by ball tip point 0 in the figure. For cutters which have constant lead length, the local helix angle is scaled by a radius factor and can be expressed as

$$\tan i(\psi) = \frac{R(\psi)}{R_0} \tan i_0 \tag{4}$$

From the equations given above, the cutter radius in the x–y plane, which touches a point on the helical and spherical flute located at angle ψ, can be expressed as

$$R(\psi) = \sqrt{1 - (\psi \cot i_0 - 1)^2} \tag{5}$$

A vector $\mathbf{r}$ is drawn from the cylindrical coordinate center (C) to a point on the cutting edge, and is defined by

$$\mathbf{r}(\psi) = R(\psi)(\sin \psi \mathbf{i} + \cos \psi \mathbf{j}) + R_0 \psi \cot i_0 \mathbf{k} \tag{6}$$

The length of an infinitesimal curved cutting edge segment dS along the ball part is computed from

$$dS = \|d\mathbf{r}\| = \sqrt{(R'(\psi))^2 + R^2(\psi) + R_0^2 \cot^2 i_0}\, d\psi \tag{7}$$

where $R'(\psi)$ is the derivative of $R(\psi)$:

$$R'(\psi) = \frac{-R_0(\psi \cot i_0 - 1) \cot i_0}{\sqrt{1 - (\psi \cot i_0 - 1)^2}} \tag{8}$$

From Fig. 1(c), the radial rake α_r and relief angle α_f are both defined in the x–y plane and the normal rake angle α_n is measured on a plane passing through the cutting point and centre of the ball, see Fig. 4. Figure 2 shows the variation of the helix angle and normal and radial rake angle in the axial direction along a flute. As formulated, the local helix angle i approaches the nominal helix angle i_0 at the ball-shank meeting point, i.e. $z = R_0$. A point on the flute j at height z is referenced by its angular position Ψ in the global coordinate system

$$\Psi_j(z) = \theta + (j - 1)\phi_p - \frac{z}{R_0} \tan i_0 \tag{9}$$

where $\phi_p = 2\pi/N_f$ is the pitch angle of the cutter and θ is the rotation of reference flute $j = 1$. θ is measured clockwise from the y-axis, and from the centre point 0. The chip

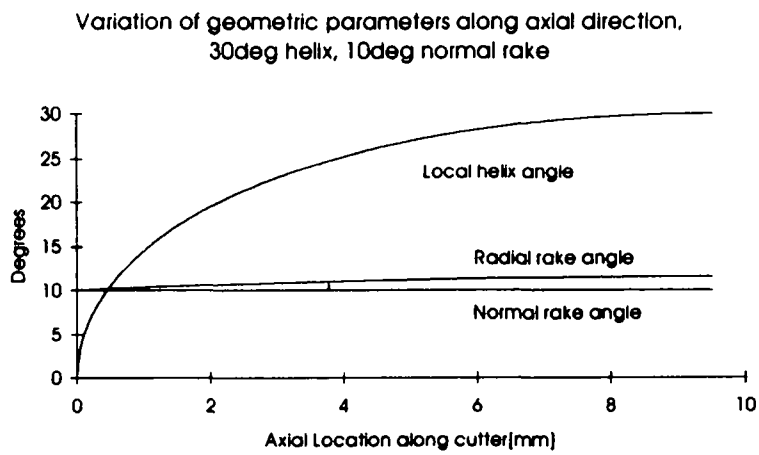

Fig. 2. Variation of local parameters along axial direction, $R_0 = 9.525$ mm, $i_0 = 30°$, $\alpha_n = 10°$.

thickness normal to the cutting edge, denoted by t_n, is a function of both the radial position angle θ and the axial angle κ as shown in Fig. 1(d),

$$t_n(\psi,\theta,\kappa) = s_t \sin(\Psi)\sin(\kappa) \tag{10}$$

where

$$\kappa = \sin^{-1}\frac{R(\psi)}{R_0} \tag{11}$$

The error introduced by the above analytical chip thickness expression is significant only in areas around the ball tip. The use of exact kinematic model of chip thickness formulated by Refs [9] and [10] did not significantly improve the results when the axial depth of cut was not too small (i.e. $a > 1$ mm).

The ball-end geometry and the helical cutting edge orientation are then used in the following section to formulate the cutting forces.

3. MODELING OF CUTTING FORCES

The geometry of a cutting edge is shown in Fig. 1(c). A set of curvilinear coordinate system normal to the ball envelope is used to specify the resultant cutting forces acting on the flute. The elemental tangential, radial, and axial cutting forces dF_t, dF_r, dF_a acting on the cutter are given by

$$\begin{aligned} dF_t(\theta,z) &= K_{te}dS + K_{tc}t_n(\theta,\psi,\kappa)\,db \\ dF_r(\theta,z) &= K_{re}dS + K_{rc}t_n(\theta,\psi,\kappa)\,db \\ dF_a(\theta,z) &= K_{ae}dS + K_{ac}t_n(\theta,\psi,\kappa)\,db \end{aligned} \tag{12}$$

where $t_n(\theta, \psi, \kappa)$ is the uncut chip thickness normal to the cutting edge, and varies with the position of the cutting point. The cutting forces are separated as edge (e) and shear cutting (c) components. The edge force coefficients (K_{te}, K_{re}, K_{ae}) are in N mm^{-1}, constant and lumped at the edge of the flutes. dS is the differential length of the curved cutting edge segment given by Equation (7). The shearing coefficients K_{tc}, K_{rc}, K_{ae} are identified from a set of orthogonal cutting tests using oblique transformation [6, 7]. They represent cutting force per unit chip area. db is the projected length of an infinitesimal cutting flute in the direction along the cutting velocity. It should be noted that db is consistent with the chip width defined in the classical oblique cutting theory. The relationship between db and dz is given by

$$db = \frac{dz}{\sin\kappa} \tag{13}$$

The resultant forces in Cartesian coordinates are obtained by introducing the transformation matrix $\mathbf{T}$

$$\{dF_{xyz}\} = [T]\{dF_{rta}\}$$

$$\begin{bmatrix} dF_x \\ dF_y \\ dF_z \end{bmatrix} = \begin{bmatrix} -\sin(\kappa)\sin(\Psi) & -\cos(\Psi) & -\cos(\kappa)\sin(\Psi) \\ -\sin(\kappa)\cos(\Psi) & \sin(\Psi) & -\cos(\kappa)\cos(\Psi) \\ \cos(\kappa) & 0 & -\sin(\kappa) \end{bmatrix} \begin{bmatrix} dF_r \\ dF_t \\ dF_a \end{bmatrix} \tag{14}$$

The total cutting forces acting on one flute with an axial depth of cut z is

$$\{F\} = \int_{z} \mathrm{d}F \tag{15}$$

where the differential force components are dependent on the flute segment length dS, instantaneous chip load $t_n(\theta, z, \kappa)$, the local rotation (θ) and lag angle (ψ).

$$\left.\begin{aligned} F_{xj}[\theta(z)] &= \int_{z_1}^{z_2} (-\mathrm{d}F_{rj}\sin(\kappa_j)\sin(V_j) \quad -\mathrm{d}F_{tj}\cos(\Psi_j) \quad -\mathrm{d}F_{aj}\cos(\kappa_j)\sin(\Psi_j))\,\mathrm{d}z \\ F_{yj}[\theta(z)] &= \int_{z_1}^{z_2} (-\mathrm{d}F_{rj}\sin(\kappa_j)\cos(\Psi_j) + \mathrm{d}F_{tj}\sin(\Psi_j) \quad -\mathrm{d}F_{aj}\cos(\kappa_j)\cos(\Psi_j))\,\mathrm{d}z \\ F_{zj}[\theta(z)] &= \int_{z_1}^{z_2} (\mathrm{d}F_{rj}\cos(\kappa_j) \qquad\qquad\qquad\qquad -\mathrm{d}F_{aj}\sin(\kappa_j))\,\mathrm{d}z \end{aligned}\right\} \tag{16}$$

Since the cutting force coefficients (K_{tc}, K_{ac}, K_{rc}) may be dependent on the local chip thickness, the integrations given above are calculated digitally by evaluating the contribution of each discrete cutting edge element at dz intervals. However, care must be taken that when the edge segment is outside the immersion zone, i.e. loss of contact with the workpiece, the contribution to the cutting forces is zero.

4. PREDICTION OF CUTTING FORCE COEFFICIENTS FROM AN OBLIQUE CUTTING MODEL

The pressure applied on the cutter due to ploughing and cutting is related to the total forces with edge force coefficients K_{te}, K_{re}, K_{ae} and cutting force coefficients K_{tc}, K_{rc}, K_{ac}. In the mechanistic approach, standard cutting tests are performed and these coefficients are identified by calibration involving least square curve fitting to experimental average force data. The identification process has to be repeated for each cutter with different geometry and the coefficients cannot be obtained prior to the machining process. In this paper, each cutting edge segment is treated as an oblique tool segment. The cutting force coefficients are evaluated from a set of orthogonal cutting tests, and transformed to oblique cutting edge geometry using classical oblique transformation model suggested by Armarego [11]. The orthogonal to cylindrical end milling cutting force transformation mechanism has been presented in Ref. [6]. A brief overview is given here which is applied to ball-end milling.

4.1. *Orthogonal cutting parameters*

A set of turning experiments resembling orthogonal cutting was conducted on titanium tubes (Ti_6Al_4V) with tools of different rake angles over different feeds and cutting speeds. The diameter of the tube was 100 mm and the cutting speed range was from 2.6 to 47 m min^{-1}. Resultant forces in the power (F_c) and thrust (F_f) directions were measured with a force dynamometer. Small steps in cutting conditions were used to increase the reliability of the measured forces. It should be noted that the measured forces may include both the forces due to shearing and a secondary process "ploughing" or "rubbing" at the cutting edge. Thus using the edge force model given in section 4, the measured force components are expressed as follows:

$$\begin{aligned} F_{Pt} &= F_{Pe} + F_{Pc} \\ F_{Qt} &= F_{Qe} + F_{Qc} \end{aligned} \tag{17}$$

The edge forces are obtained by extrapolating the measured forces to zero chip thickness. From Fig. 3 it can be seen that the edge forces do not vary significantly with cutting speeds and rake angles for the particular workpiece material used here. The average edge force coefficients K_{tc}, K_{re}, K_{ae} represent the rubbing forces per unit width and are obtained by integrating the in-cut flute length [dS in Equation (7)] numerically. The K_{ae} value is usually small and taken as zero [7].

The chip compression ratio (r), shear stress τ, shear angle θ and friction angles are calculated from the measured "cutting" component of the forces and the cutting ratio by applying the orthogonal cutting theory presented in Ref. [12].

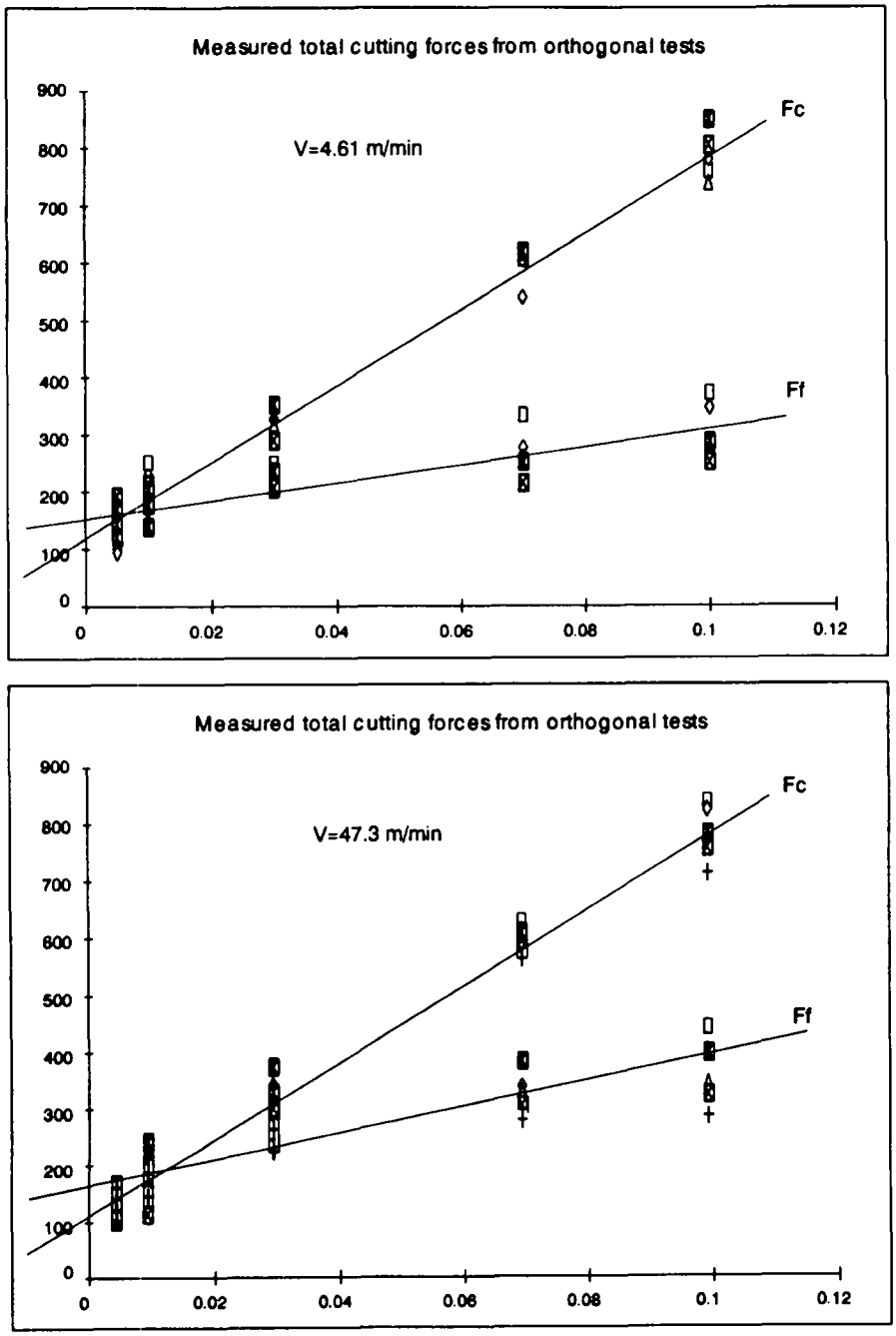

Fig. 3. Edge forces extrapolation from orthogonal machining tests.

$$\left.\begin{aligned} \tau &= \frac{(F_{Pc}\cos\phi - F_{Qc}\sin\phi)\sin\phi}{bt} \\ \tan\phi &= \frac{r\cos\alpha}{1 - r\sin\alpha} \\ \tan\beta &= \frac{F_{Qc} + F_{Pc}\tan\alpha}{F_{Pc} - F_{Qc}\tan\alpha} \end{aligned}\right\} \tag{18}$$

The fundamental machining parameters—the shear stress (τ), average friction angle β, chip compression ratio r—are estimated by employing a least square curve fitting technique to the measured orthogonal test results. The identified relationships are summarized in Table 1. From the results it is observed that the shear stress does not vary significantly with either the rake angle or the cutting speed. The cutting ratio, however, depends slightly on the uncut chip thickness. The average friction angle on the rake face is expressed as a function of the rake angle. These relationships are valid only for the particular workpiece material (Ti_6Al_4V) tested here, and other materials may exhibit different relationships.

4.2. *Oblique cutting*

Ball-end mill flutes are treated as combination of series of oblique cutting edge segments. An oblique cutting geometry based on the thin shear zone model is shown in Fig. 4. The chip velocity V_c is inclined at an acute angle i to the plane P_n normal to the cutting edge. Using Merchant's theory, resolving the resultant forces due to "cutting" on the shear plane into three mutually perpendicular components yields [6, 11]

$$\begin{aligned} F_p &= \frac{\tau bt}{\sin\phi_n}\,\frac{\cos(\beta_n - \alpha_n) + \tan\eta_c\sin\beta_n\tan i}{c} \\ F_q &= \frac{\tau bt}{\sin\phi_n\cos i}\,\frac{\sin(\beta_n - \alpha_n)}{c} \\ F_r &= \frac{\tau bt}{\sin\phi_n}\,\frac{\cos(\beta_n - \alpha_n)\tan i - \tan\eta_c\sin\beta_n}{c} \end{aligned} \tag{19}$$

where

$$c = \sqrt{\cos^2(\phi_n + \beta_n - \alpha_n) + \tan^2\eta_c\sin^2\beta_n}$$

F_p, F_q, F_r are the power, thrust and radial forces acting on the oblique cutting edge segment, respectively. The normal friction angle, β_n, is defined as

$$\tan\beta_n = \tan\beta\cos\eta_c \tag{20}$$

where β is the average friction angle at the rake face of an orthogonal cut and η_c is the chip flow angle (the angle between a perpendicular to cutting edge and the direction of chip flow over rake face, as measured in the plane of tool face). The normal rake angle

Table 1. Orthogonal cutting data

$\tau = 613$ MPa
$\beta = 19.1 + 0.29\alpha$
$r = r_0 t^a$
$r_0 = 1.755 - 0.028\alpha$
$a = 0.331 - 0.0082\alpha$
$K_{te} = 24$ N mm^{-1}
$K_{re} = 43$ N mm^{-1}

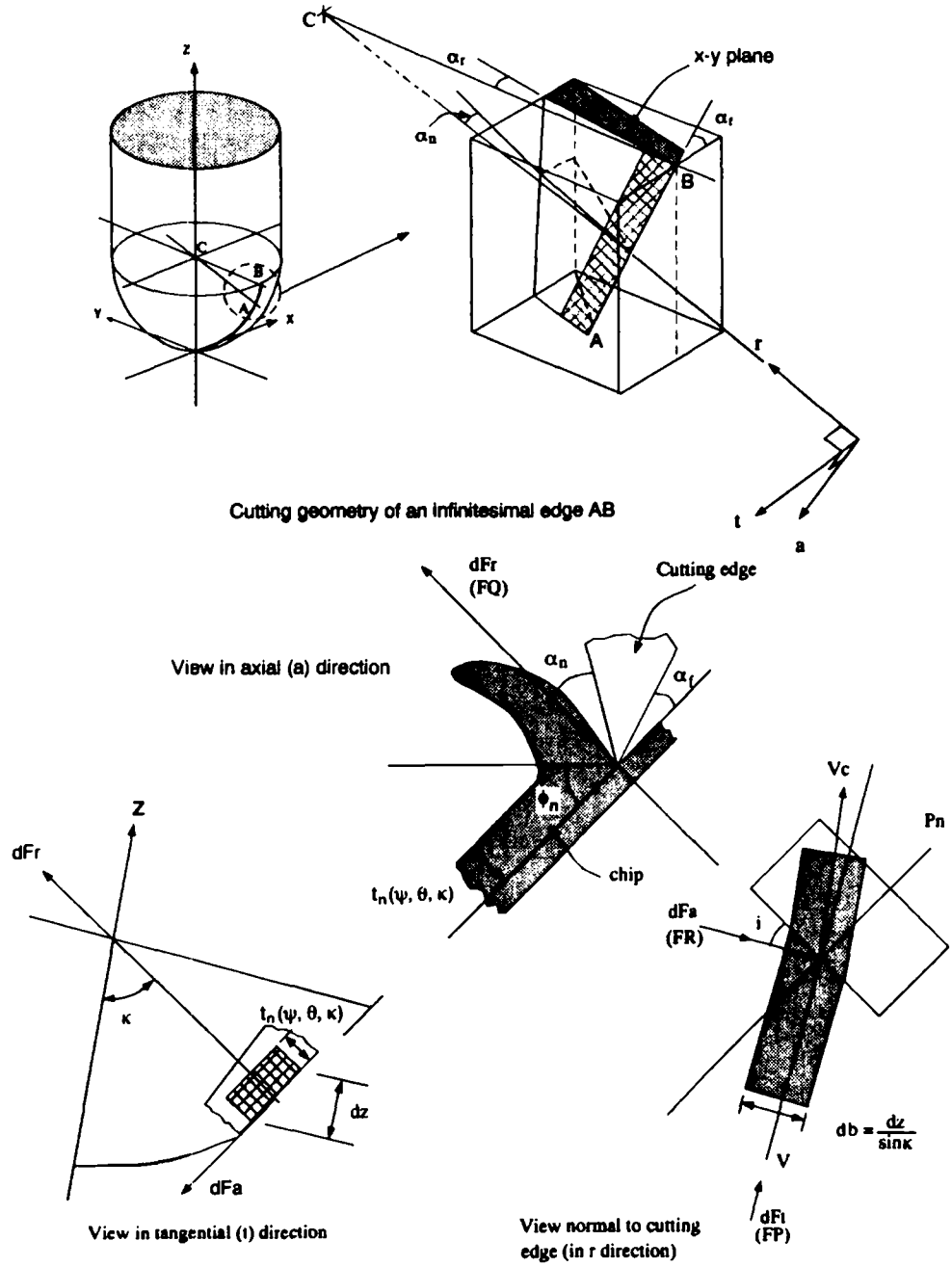

Fig. 4. Oblique cutting geometry.

is constant, and set during cutter grinding as shown in Fig. 4. The normal shear angle, ϕ_n, is obtained from the cutting ratio

$$\tan\phi_n = \frac{r_t \cos\alpha_n}{1 - r_t \sin\alpha_n} \tag{21}$$

r_t is the chip thickness ratio in oblique cutting and is related to orthogonal parameter r by $r_t = r\dfrac{\cos\eta_c}{\cos i}$. This relation is obtained from the mass continuity equation of the chip before and after the cut. To further simplify the model, the Stabler rule is applied in which the chip flow angle η_c is approximated by the local inclination angle i [13]. From Fig. 4

in which a small segment on the ball-end cutter is shown, the tangential, radial and axial force components dF_t, dF_r, dF_a are compatible with the power, thrust and radial force components F_p, F_q, F_r, in oblique cutting when the elemental cut thickness t and width of cut b are given by the instantaneous chip thickness $t_{nj}(\psi, \theta, \kappa)$ and length $dz/\sin(\kappa)$ [7]. Thus the milling force component coefficients due to "cutting" in Equation (1), i.e. K_{tc}, K_{rc} and K_{ac}, can be expressed in terms of the transformed cutting coefficients.

$$K_{tc} = \frac{\tau}{\sin\phi_n} \frac{\cos(\beta_n - \alpha_n) + \tan\eta_c \sin\beta_n \tan i}{c}$$

$$K_{rc} = \frac{\tau}{\sin\phi_n \cos i} \frac{\sin(\beta_n - \alpha_n)}{c} \tag{22}$$

$$K_{ac} = \frac{\tau}{\sin\phi_n} \frac{\cos(\beta_n - \alpha_n)\tan i - \tan\eta_c \sin\beta_n}{c}$$

Cutting pressures in tangential, radial and axial directions are calculated locally along

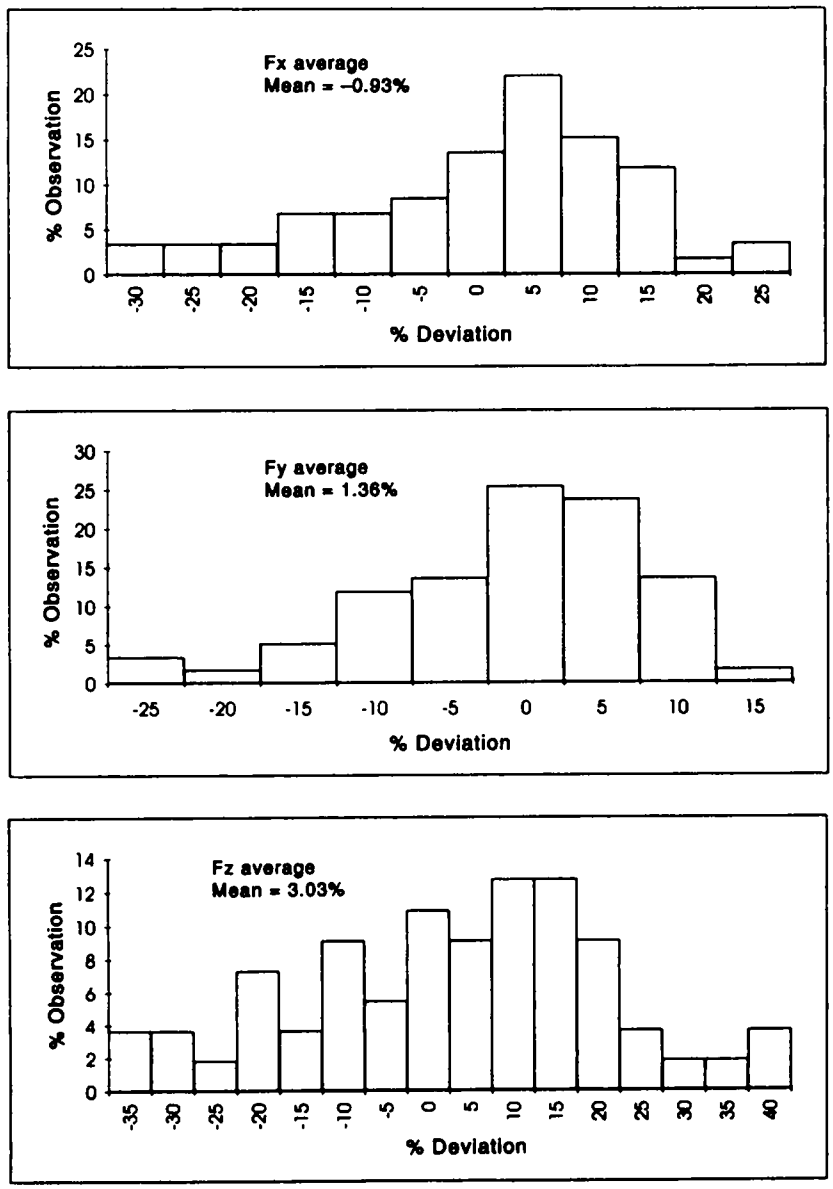

Fig. 5. Statistical evaluation of model and data.

Table 2. Cutting conditions for tests and simulations

R_0 = 6.35, 9.525 mm
α_n = 0–15°
i_0 = 30°
N_f = 1
s_t = 0.0127–0.127 mm tooth^{-1}
a = 1.27–8.89 mm
N = 269 rpm

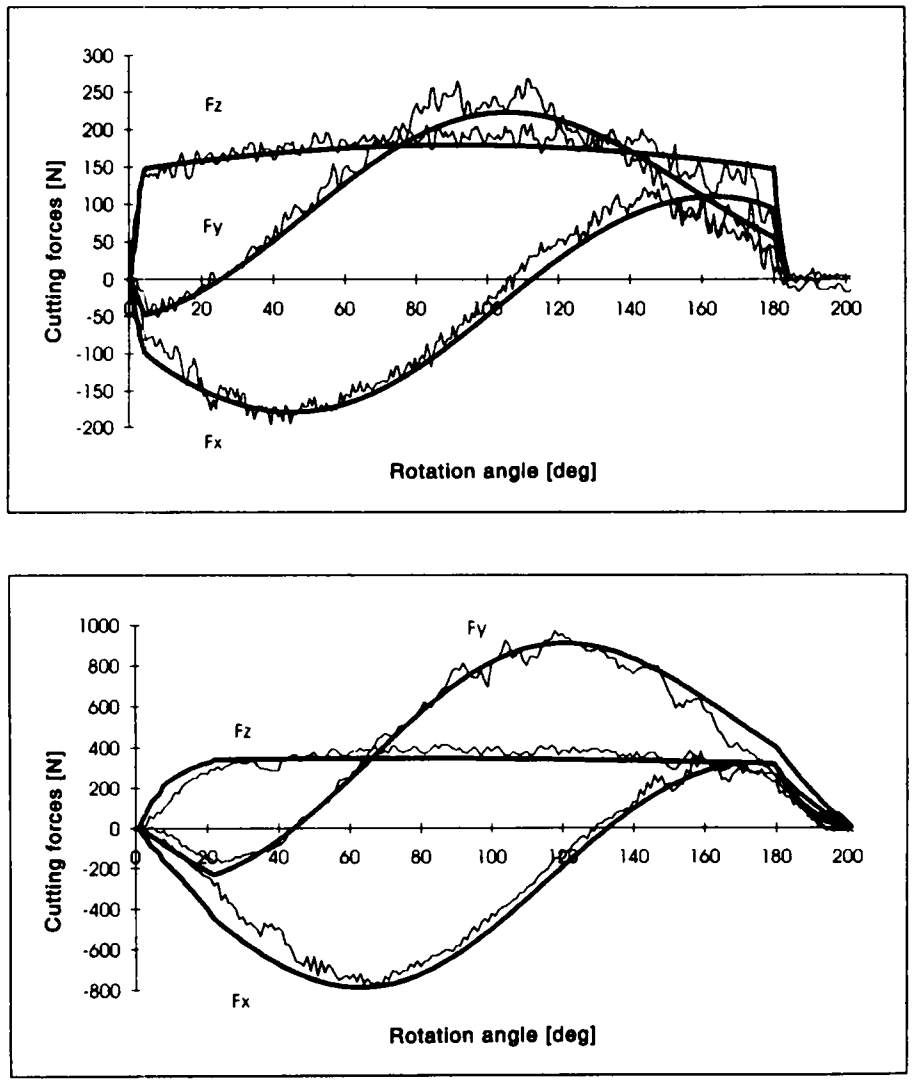

Fig. 6. Measured and predicted cutting forces for slot cutting tests, α_n = 0°, spindle speed = 269 rev min^{-1}, R_0 = 9.525 mm, i_0 = 30°, s_t = 0.0508 mm flute^{-1}: (a) a = 1.27 mm; (b) a = 6.35 mm.

each cutting flute segment, and elemental forces are summed along each cutting edge to evaluate the final cutting forces.

5. SIMULATION AND EXPERIMENTAL VERIFICATION

More than 60 cutting tests were conducted on a vertical CNC milling machine with 30° nominal helix, single flute, carbide ball-end mills. Slot cutting experiments were selected on a titanium alloy (Ti_6Al_4V) at different feeds and axial depth of cuts with cutter rake angles ranging from 0 to 15°. Cutters with two different radius were used (6.35 and 9.525 mm). The tests were conducted without lubricant and the forces were measured

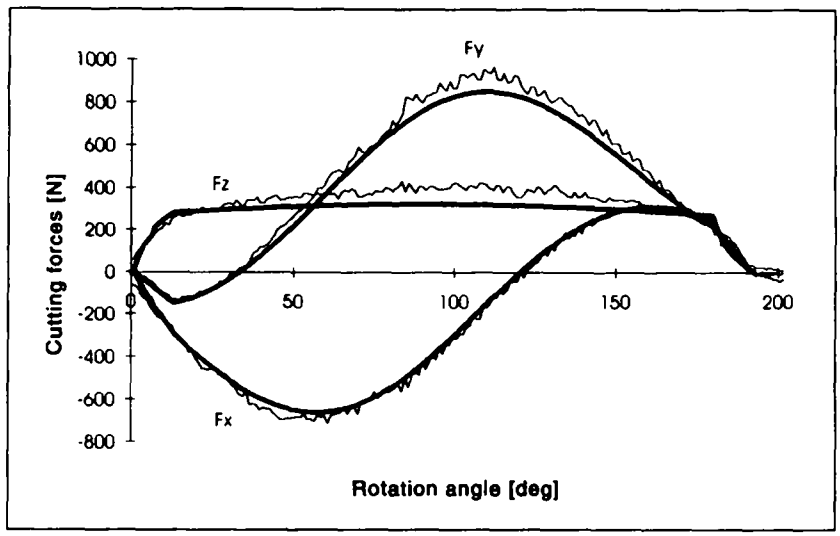

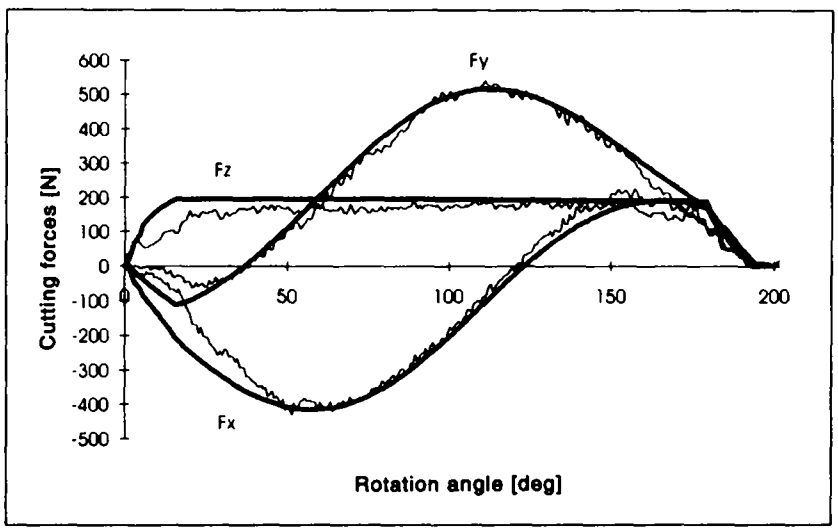

Fig. 7. Measured and predicted cutting forces for slot cutting tests, spindle speed = 269 rev min^{-1}, $i_0 = 30°$: (a) a = 3.81 mm, R_0 = 9.525 mm, s_t = 0.1016 mm flute $^{-1}$, rake=5; (b) a = 3.048 mm, R_0 = 6.35 mm and s_t = 0.0762 mm $flute^{-1}$, rake = 10.

with a three-component Kistler table dynamometer. Cutting conditions for the tests and simulations are summarized in Table 2.

The solution of Equation (16) can be obtained by applying a numerical integration technique. The cutter is first discretized axially into small discs with different radii, the lag angle of the flute j at height z in a global coordinate is given in Equation (9).

At any tool rotation angle θ, it is first checked whether the flute is in or out of cut. For example, in half immersion up-milling the flute segment k is in cut if $(\psi_k)_j > 0$ and $(\psi_k)_j < \pi/2$.

The forces for multiple fluted cutters are obtained by summing the forces acting on the individual flutes in-cut.

Using the predictive force model with classical orthogonal cutting machining parameters, the simulation and experimental results were compared. The percentage difference between the predicted and experimental results has been used to evaluate the statistical reliability of the model.

Figure 5 shows the histograms of the percentage errors and the mean values of the average forces. It can be seen that the model provides sound predictions of the cutting

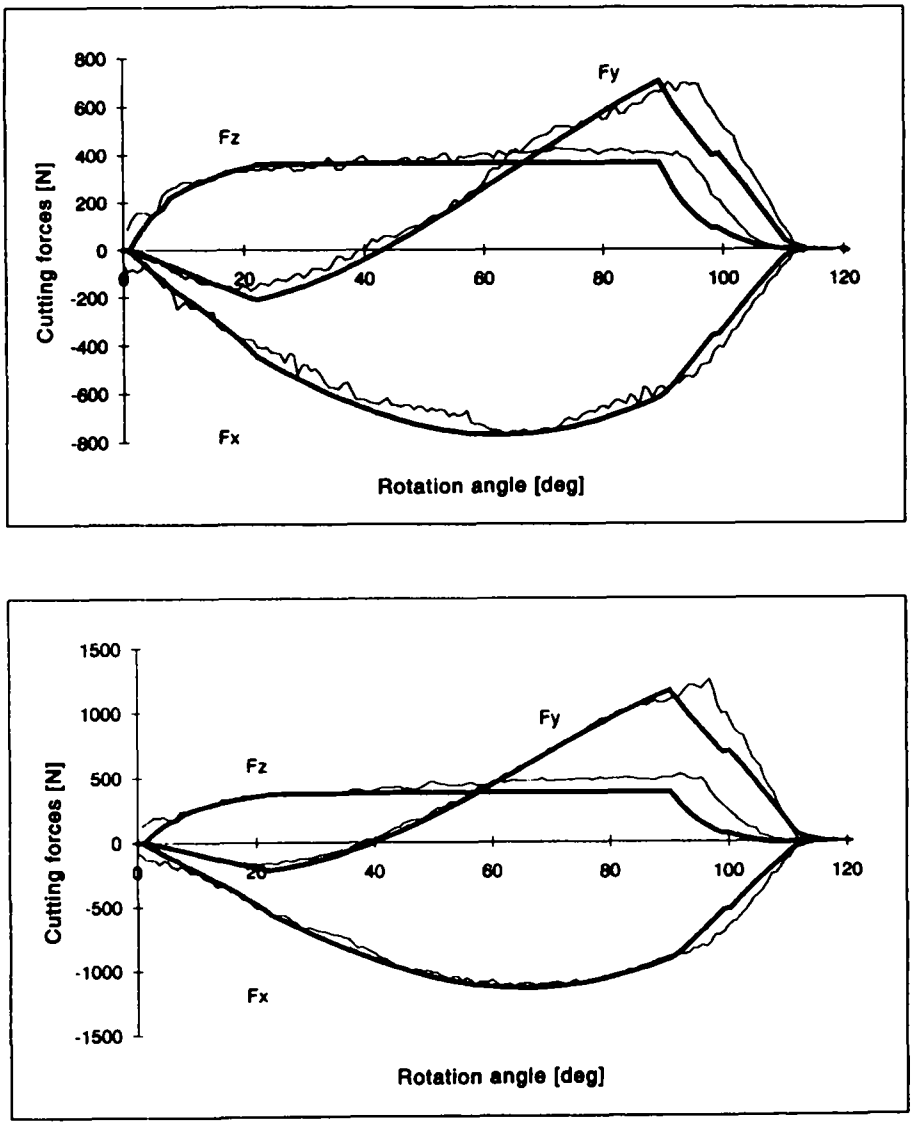

Fig. 8. Measured and predicted cutting forces for half radial immersion cutting tests, $\alpha_n = 0°$, $a = 6.35$ mm, spindle speed = 269 rev min^{-1}, $i_0 = 30°$: (a) $s_t = 0.0508$ mm flute^{-1}; (b) $s_t = 0.102$ mm flute^{-1}.

forces in all three components qualitatively and quantitatively, with a mean deviation of -0.93% for average F_x, 1.36% for average F_y and 3.03% for average F_z. The corresponding ranges in percentage deviation are -30–25% for average F_x, -25–15% for average F_y and -35–40% for average F_z. In Fig. 6 a sample simulation of cutting forces for a slotting test with axial depth of cuts $a = 1.27$ and 6.35 mm at feed-rate $f_d = 0.0508$ mm are shown for a single fluted cutter with zero rake angle. The cutting force pattern in the axial direction is dominated by the ploughing action between the flute and the material. As soon as the flutes enter into the cut, the flank forces develop rapidly while the chip thickness is still small. In Fig. 7, predicted and measured cutting forces for a slotting test with different sizes of cutters are shown. The predicted and simulated cutting forces are in good agreement. In a separate case, half immersion up-milling tests with axial depth of cut $a = 6.35$ mm with two different feed-rates of $f_d = 0.0508$ and 0.1016 mm rev^{-1} were conducted. Again the predicted and measured cutting forces, as seen in Fig. 8, are in good agreement except with slight phase shifts at the exit due to difficulty in selecting the reference point in the half immersion test data.

6. CONCLUSIONS

The prediction of cutting forces in ball-end milling operations is presented. The model is based on the establishment of a data base containing basic machining quantities evaluated from a set of standard orthogonal cutting tests. Later, the orthogonal cutting test data base is used to calculate corresponding oblique cutting force parameters. Using the geometry and kinematics of the ball-end milling process, the cutting forces in three directions are predicted accurately. The paper demonstrates that when fundamental orthogonal cutting parameters of a material are stored in a data base, milling forces produced by complex ball-end mills can be predicted having to mechanistically calibrate milling cutters prior to their design. The approach should be helpful to cutter design and process planning engineers.

Acknowledgements—This research is jointly supported by the Natural Science and Research Council of Canada and Pratt and Whitney Canada under a co-operative Research and Development grant titled "Peripheral milling of titanium based jet engine compressors". The grant number is NSERC CRD0045998. The authors gratefully acknowledge Pratt and Whitney Canada who supplied the tools and titanium material for the cutting tests.

REFERENCES

[1] E. M. Lim, H. Y. Feng and C. H. Menq, The prediction of dimensional errors for machining of sculptured surfaces using ball-end milling, *ASME Winter Ann. Meet*, New Orleans, U.S.A., PED-Vol. 64, pp. 149–156 (1993).
[2] G. Yucesan and Y. Altintaş, Mechanics of ball end milling process, *ASME Winter Ann. Meet*, New Orleans, U.S.A., *Proc. Mfg Sci. Engng* PED-Vol. 164, pp. 543–551 (1993)
[3] M. Yang and H. Park, The prediction of cutting force in ball end milling, *Int. J. Mach. Tools Manufact.* **31**(1), 45–54 (1991).
[4] C. Sim and M. Yang, The prediction of the cutting force in ball end milling with a flexible cutter, *Int. J. Mach. Tools Manufact.* **31**(2), 267–284 (1993).
[5] C. C. Tai and K. H. Fuh, A predictive force model in ball-end milling including eccentricity effects, *Int. J. Mach. Tools Manufact.* **34**(7), 959–979 (1994).
[6] E. Budak, Y. Altintas and E. J. A. Armarego, Prediction of milling force coefficients from orthogonal cutting data. *Trans. ASME J. Engng Ind.* (in press).
[7] E. J. A. Armarego and R. C. Whitfield, Computer based modeling of popular machining operations for forces and power prediction, *Ann. CIRP* **34**(1), 65–69 (1985).
[8] T. C. Ramaraj, Analysis of the mechanics of machining with tapered end milling cutters, *Trans. ASME*, JEI-Vol. 116, pp. 398–404 (1994).
[9] M. Martelotti, Analysis of the milling process, *Trans. ASME* **63**, 667 (1941) and **67**, 233 (1945).
[10] D. Montgomery and Y. Altintaş, Mechanism of cutting force and surface generation in dynamic milling, *Trans. ASME J. Engng Ind.* **113**, 160–168 (1991).
[11] E. J. A. Armarego and R. H. Brown. *The Machining of Metals*. Prentice Hall, New York (1969).
[12] M. E. Merchant, Basic mechanics of metal cutting process, *Trans. ASME J. Appl. Mech. A* 168–175 (1944).
[13] G. V. Stabler, Fundamental geometry of cutting tools, *Proc. Instn Mech. Engrs*, 14–26 (1951).